NASA / DLR Design Challenge 2019

Xargo Aircraft Concept

Team
B. Çetinoğlu, M.Y. Cürebal, A. Gatto, A. Gebhardt, J. Oppe, D. Roßner

Academic Support
Dipl.-Ing. Florian Dexl
Chair of Aircraft Engineering
TU Dresden

Submission Date
July 1st, 2019

Team Members

Team members from left to right:

Daniel Roßner
Aeronautical Engineering, 6th semester (Diploma)
daniel.rossner@mailbox.tu-dresden.de

Johannes Oppe
Aeronautical Engineering, 10th semester (Diploma)
johannes.oppe@mailbox.tu-dresden.de

Anne Gebhardt
Mechanical Engineering, 10th semester (Diploma)
anne-lisa.gebhardt@mailbox.tu-dresden.de

Mustafa Yasar Cürebal
Aeronautical Engineering, 8th semester (Bachelor)
mustafa_yasar.cuereball@mailbox.tu-dresden.de

Bengisu Çetinoğlu
Aeronautical Engineering, 8th semester (Bachelor)
bengisu.cetinoglu1@mailbox.tu-dresden.de

Arnold Gatto (Team Lead)
Aeronautical Engineering, 10th semester (Diploma)
arnold.gatto@mailbox.tu-dresden.de

TECHNISCHE UNIVERSITÄT DRESDEN

Fakultät für Maschinenwesen Institut für Luft- und Raumfahrttechnik

Declaration of Authorship

We hereby declare that the thesis submitted is our own unaided work. All direct or indirect sources used are acknowledged as references.

We are aware that the thesis in digital form can be examined for the use of unauthorized aid and in order to determine whether the thesis as a whole or parts incorporated in it may be deemed as plagiarism.

This paper was not previously presented to another examination board and has not been published.

Dresden, July 1st, 2019

TECHNISCHE UNIVERSITÄT DRESDEN

Fakultät Maschinenwesen Institut für Luft- und Raumfahrttechnik

Technische Universität Dresden, 01062 Dresden

Deutsches Zentrum für Luft- und Raumfahrt e. V. (DLR)
Institut für Systemarchitekturen in der Luftfahrt | Flugzeugentwurf & Systemintegration

Prof. Dr.-Ing.
Klaus Wolf
Lehrstuhl für Luftfahrzeugtechnik

Bearbeiter: Florian Dexl

Telefon: 0351 463-38096
Telefax: 0351 463-37263
E-Mail: florian.dexl@tu-dresden.de
AZ: 19-52

28/06/2019

NASA/DLR Design Challenge: Approval and support of report submission

To whom it may concern,

As the academic supervisors, we hereby declare to approve the report written by the student team consisting of

- Bengisu Çetinoğlu,
- Mustafa Yaşar Cürebal,
- Arnold Gatto,
- Anne Gebhardt,
- Johannes Oppe,
- Daniel Roßner

and support the submission to the NASA/DLR Design Challenge 2019. We further declare that the report is the result of the above-listed students' own work.

Best regards

TECHNISCHE UNIVERSITÄT DRESDEN
Institut für Luft- und Raumfahrttechnik
Lehrstuhl für Luftfahrzeugtechnik
Prof. Dr.-Ing. Klaus Wolf
01062 Dresden

Prof. Dr.-Ing. K. Wolf Dipl.-Ing. Florian Dexl

Abstract

Commercial Operation of small aircraft poses a major challenge for airliners as they are faced with a number of economic difficulties. Especially in remote areas flight missions are characterized by short-haul distances with low demand and consequently high takeoff und landing frequencies in relation to the total flight hours leading to excessive fix costs and direct operation costs for the air carrier. However, accessibility of remote regions are essential as they often are the only possible connection for local communities to reach nearest cities.

To address above mentioned economic issues the TU Dresden student team has come up with a design proposal of an aircraft concept aiming to surpass contemporary commuter airplanes in efficiency and overall economy. The present report provides an overview of the Design Layout and demonstrates compliance with a set of Top Level Aircraft Requirements (TLAR) established within the 2019 NASA / DLR Design Challenge along with regulatory requirements of the Federal Aviation Administration. Furthermore, integrated key technologies are explained and assessed with respect to credibility of 2025 entry into service. For this purpose the commonly known Technology Readiness Level (TRL) is estimated accordingly.

Xargo is a nine-seated high wing commuter aircraft equipped with two electrically driven propeller designed for cruise flight and two additional tiltable rotors enabling short take-off and landing capability and generous rate of climb. The required amount of energy is converted by a hydrogen fuel cell providing all four electric motors with adequate power. By means of a modular cockpit and payload compartment design the aeroplane is suitable for quick conversion between passenger and unmanned cargo operation. Comparison with existing commuter planes show significant savings in costs due to improved aerodynamics, sophisticated propulsion strategy and light weight composite structure.

Contents

Nomenclature

Symbol	Description	Unit
Abbreviations		
EAS	Essential Air Service, Equivalent Air Speed	
FAA	Federal Administration of Aviation	
CAD	Computer Aided Design	
CAS	Callibrated Air Speed	
CFR	Code of Federal Regulations	
CFRP	Carbon Fiber Reinforced Plastics	
CoG	Center of Gravity	
DC	Design Challenge	
DOC	Direct Operating Costs	
DGTW	Design Takeoff Gross Weight	
GPS	Global Positioning System	
GBAS	Ground Based Augmentation System	
ICA	Initial Cruise Altitude	
ILS	Instrument Landing System	
MZFM	Minimum Zero Fuel Mass	
OLED		
PEFC	Polymer Electrolyte Fuel Cell	
STOL	Short Takeoff and Landing	
UAS	Unmanned Air System	
TLAR	Top Level Aircraft Requirements	
TRL	Technology Readiness Level	
WTE	Wing Tip Engine	
XME	Xargo Main Engine	
Greek		
α	angle of attack	rad,°
η	efficiency	–
Φ_F	volume density of carbon fiber in composite	–
Latin		
D	drag force	N
e	mass specific energy	kJ/kg
E	Energy	J
L	lift force	N
m	mass	kg
p^*	mass specific power	kW/kg
P_m	mass specific power density	kW/kg
P_v	volume specific power density	kW/kg
R_{II}	breaking stress composite	N
t	thickness	mm
T	thrust	N
Indices		

max	maximum
min	minimum
fc	fuel cell

List of Figures

List of Tables

1 Introduction

1.1 Background

It is no surprise that commercial operation of small aircraft is quite a challenging task from an airline's point of view. As the number of seats goes down and flight hours decrease, fix costs rise tremendously. Furthermore, higher than average expenses on maintenance and fuel arise leading to an incline in direct operating costs (DOC). This is primarily caused by frequent takeoffs and landings in relation to total flight hours, demanding sooner inspections at increasing intervals.

To counteract the tendency of airliners to shift their operation to potentially more lucrative markets, the United States Department of Transportation established the Essential Air Service (EAS). Within this programme the government subsidizes certified air carriers to serve approximately 175 communities in nearly every state that otherwise would not be able to get access to any scheduled flight service [1].

However, a close look into America's largest commuter airline's route distribution (see Figure 1) indicates that it cannot rely solely on government grant. 55% of their flights do not meet the requirements of the Department of Transportation to qualify for EAS. A fleet of highly efficient aircraft that operate within distances of 100 NM or less is therefore crucial for the airline's profitability. *Cape Air* estimates that 11,000 nine-seated aircraft need to be replaced in the near future as the majority of the current world-wide fleet is not capable of commercial operation anymore [2]. Hence, one can conclude that there is vast necessity for the aircraft industry to come up with more innovative and more importantly more economical concepts of short-haul commuter planes.

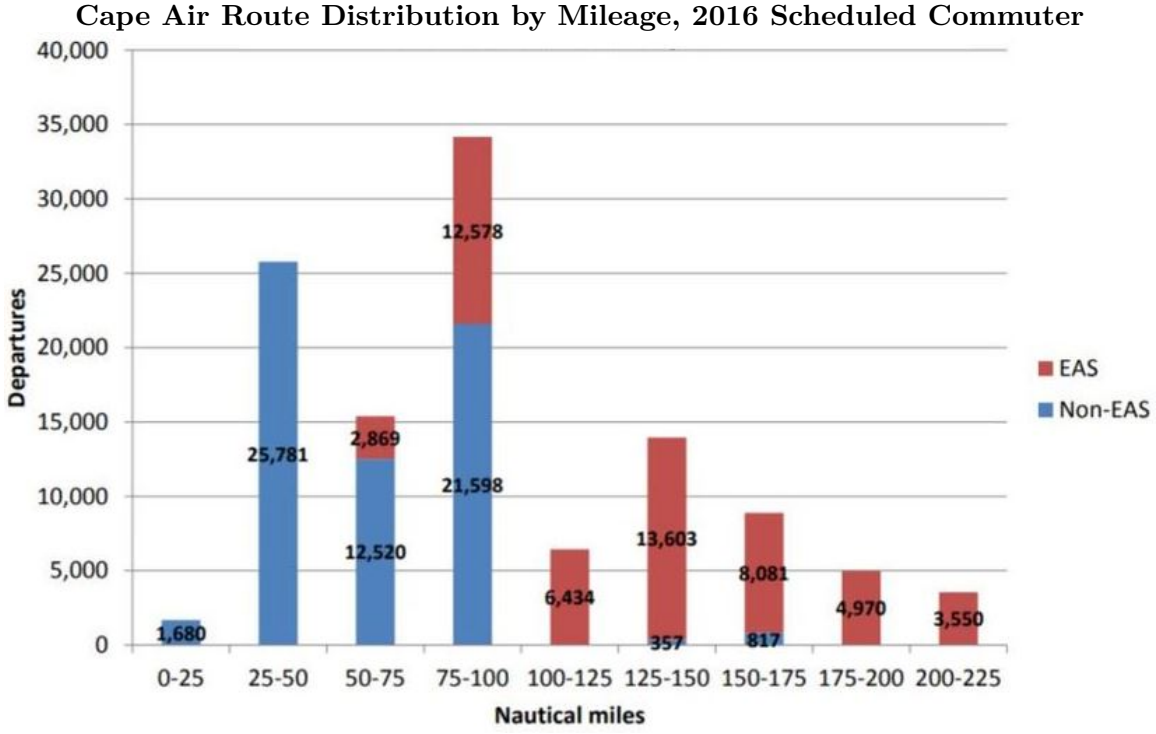

Figure 1: Route Distribution of Commuter Airline *Cape Air* from [2]

NASA and DLR have specified their perception of the next generation commuter aircraft by a list of requirements and characteristics that may be summarized as:

- short takeoff and landing capability,
- convertable between passenger and cargo configuration in less than one hour,
- unmanned freight operation,
- low noise emission,
- low life cycle cost,
- compliance with 14 CFR Part 135 and Part 23.

1.2 Existing nine-seated Commuter Planes

The current fleet of commuter aircraft with approximately nine seats involve models of manufacturers like *Cessna*, *Pilatus*, *Piper* or *Beechcraft*. Table 2 compares the most well-known representatives by their specifications. Like the *Cessna 402C* or *Pilatus PC-12* the majority of the commuter planes were built in the last century and, as the author of [3] points out, are not optimized for short-haul operation. After all, as figure 1 indicates, 67% of *Cape Airs* flights are less than 100 NM. Recently, the Italien company *Tecnam* has built their *P2012 Traveller* which is expected to entry service this year. With relatively short runway length it gets probably the closest to the requirements of the 2019 NASA / DLR Design Challenge (DC). However, its piston engines do not provide sufficient power to reach the possible range in less than 99 minutes which is a major design driver as it restricts the effective range a commuter aircraft without lavatory onboard can operate in. Furthermore, all contemporary planes in this category still rely on conventional power supply whereas particularly small aircraft might benefit the most of alternative propulsion concepts.

	Cessna 402C	Pilatus PC-12	Tecnam P2012	DC 2019 (Goal)
Range	875 NM	1,845 NM	620 NM	500 NM
Max Cruise Speed	194 KTAS	285 KTAS	210 KTAS	>320 KTAS
Takeoff Run	1,763 ft	1,480 ft	1,410 ft	250 ft
Seats	10	11	11	9
Entry into Service	1967	1994	2019	2025

Table 2: Specification of similar Commuter Aircraft (Data from [3])

1.3 Tools and Methods

Most of presented calculations are based upon handbook methods suggested by aircraft engineer and author Daniel P. Raymer. These include both empirical formulae and statistical interpolations as well as simple analytical equations. For flight performance calculations, teaching material provided by TU Dresden Professor K. Wolf, head of aircraft engineering was a main source. Underlying analytical models, assumptions and their limitations are discussed in chapter 4.

Aircraft conceptual design is a strongly iterative process that requires frequent changes especially until the final configuration is chosen. This is why a parametric computer model was built first before using any computer aided design (CAD) software for more sophisticated design features. NASA's open source software OpenVSP has been of tremendous use as it allows for quick and uncomplicated change in aircraft geometry. Performance calculations were made using spreadsheet software such as *Excel* as well as *Mathcad*. *Catia V5* was used for CAD modelling of the final aircraft design and rendering.

2 Design Overview

2.1 Design Layout

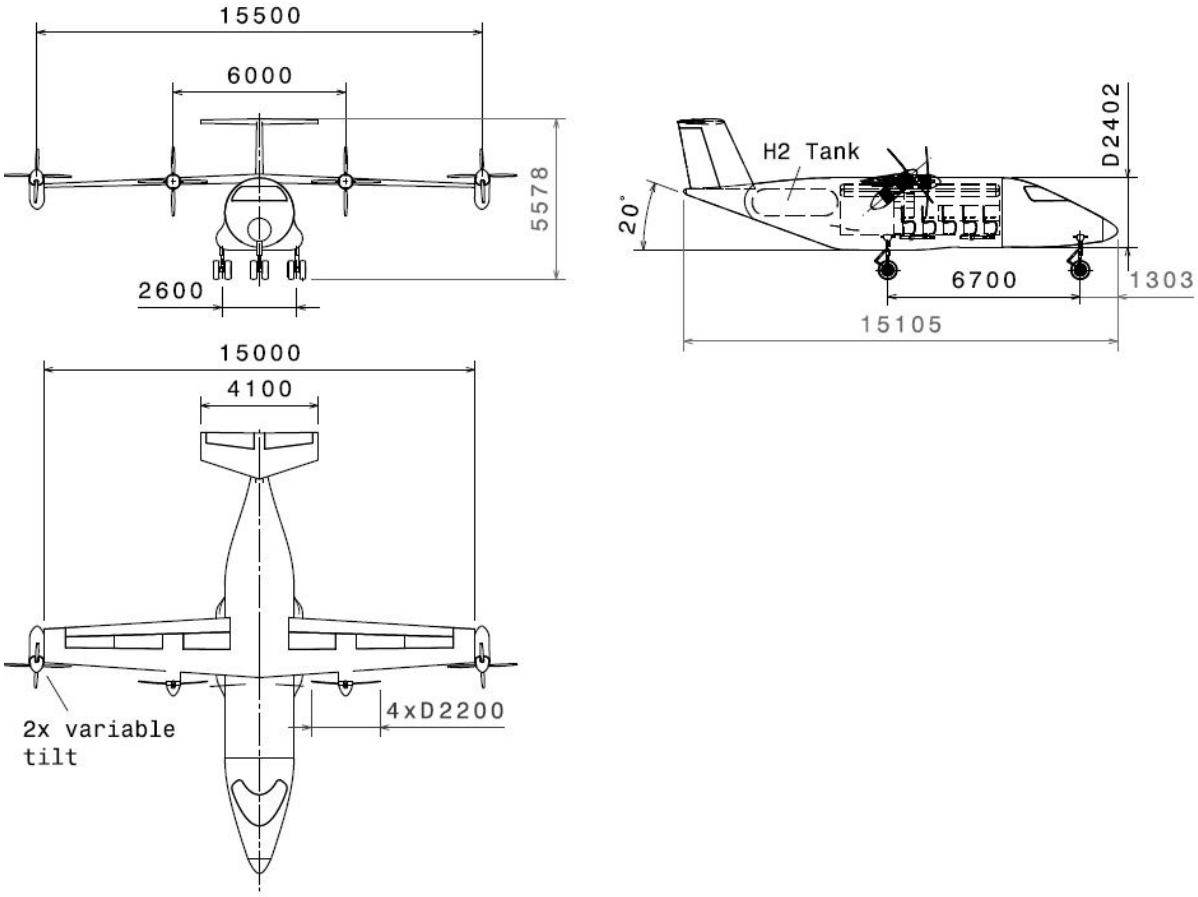

Figure 2: Multiview Orthographic Projection

2.1.1 Fuselage

When looking at *Xargo's* fuselage two things in particular stand out that is not seen very often. Firstly, there are no windows for the passengers to look out and secondly, there are is no door to enter the aircraft. Windows might still be necessary for long range flight, for missions of 120 NM distance however, the view outside can be replaced by state-of-the-art transmission technology that monitors the instantaneous scenery on 180° OLED displays covering the walls around the passenger. This drastically simplifies manufacturing of the fuselage tube made from carbon fibre reinforced plastics (CFRP) and allows for a more weight saving oriented design as there are no holes that reduce the fuselage's stiffness.

The access to the interieur of the aircraft is realized by a swivel mechanism between the cockpit and the passenger section. Figure 3 schematically illustrates how this may be done. For stability, a lever is extended to the ground supporting the joint during the opening movement. This way the nose section can open sideways. The main advantage of this particular design feature is that it allows for autonomous loading and unloading of both freight and passengers in a modular manner. Boarding procedure is explained in greater detail in section 3.1

Figure 3: Swivel Mechanism

Both cockpit and payload compartment are separate entities. They are basically enclosed containers that are detachable of the fuselage structure at any time. Figure 4 exemplarily shows such a module for the passenger cabin. There are also containers like this for cargo on freighter missions as well as for the cockpit, respectively. As seen in Figure 4, the cabin consists of a single aisle and two seating rows allowing occupation of 9 passengers. Additionally, design comparisons to already existing small airplanes had been drawn to confirm the design choice. The option of a single aisle, single seat row had been considered due to aerodynamic benefits, however it was not expected to fullfill enough stability considering the bending moment caused by the wings. Enough space is provided within the fuselage for the passengers luggage in the cabinet behind the seating row on the left-hand side of the aisle. Carry-On (seizing a maximum of 9 x 14 x 22 inch) can be stored there. For Check-In luggage (seizing a maximum of 36 x 16 x 28 inch) the remaining space behind the cabinet is used. Here, tension belts secure the luggage during flight. Futhermore, the choice was made to exclude head compartments in order to gain head space which increases passenger comfort. To provide a view and hence further comfort, passengers are surrounded by an OLED wall. Using live-cameras, passengers are able to see the sky during the flight. It is expected due to fast technology development in photonics [4] and industries investment projection [5], that OLED screens will be extra slim and affordable in the near future. Instead of the outside view transmission there are endless possibilities to display, for instance sun set ambience or even aquarium scenery. The decision in this regard is up to the operating company. The slim design of the seats was chosen because of the narrow cabin. Furthermore, the design allows passengers to appreciate the projected view of the OLED screens. The seats are expected to fullfill the restrictions of the FAAs security standards. The emergency exit for both passengers and pilot will be one of the cockpit windows. Doors and openings in the modules

that may be operated without effort ensure the accessibility for everyone onboard. In case of an emergency, the designated window slides open by simply pressing a button next to the pilots head. A rope is provided for passengers to let themselves down the nose safely. Also, a life-jacket is provided for every passenger which is part of an emergency kit that is stored underneath the seat.

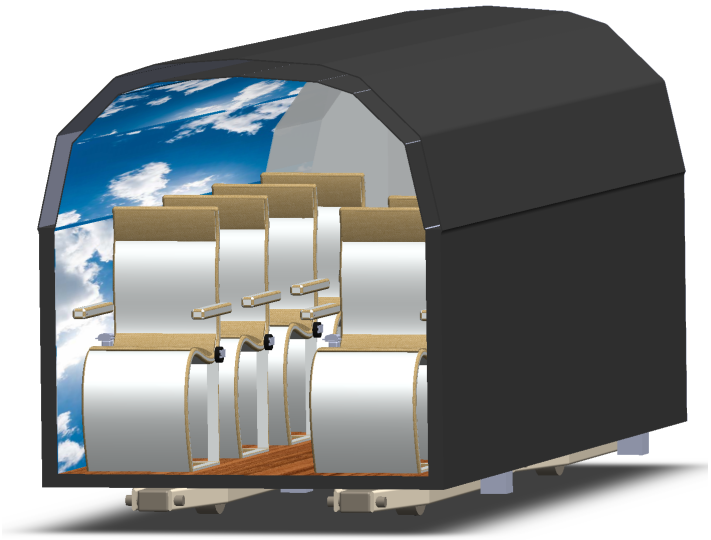

Figure 4: Passenger Cabin Module

The cross section of *Xargo* is of circular shape. In figure 5 one can see reason why this kind of cross section was chosen. The space between the cabin module and the fuselage skin is used to store additional hydrogen tanks and the required fuel cell packages.

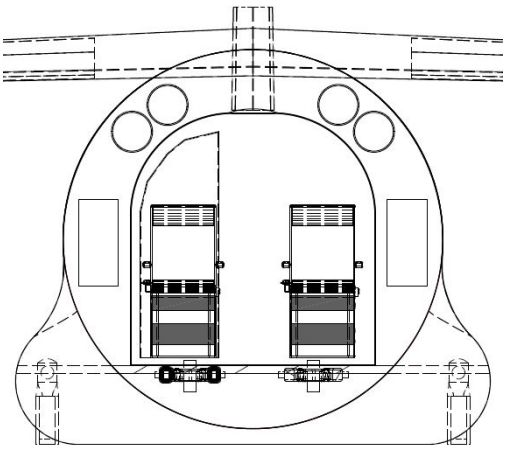

Figure 5: Fuselage Cross Section

2.1.2 Wing

Since *Xargo* will mainly serve in rural regions where takeoff and landing takes place at mostly unpaved airstrips, stones flying around or dirt hitting the propeller or engines are a concern that should not be neglected in the design of the aircraft. Therefore, the choice was made to place the wing above the fuselage. This allows for shortening the landing gear since there is

no crucial floor clearance requirement to consider which also facilitates loading and unloading precedure.

The required STOL capability is a major design driver when it comes to conceptualizing the wing. Because of the tilt of the outer engines both wing area and maximum lift coefficient are still at moderate amounts which favours cruise efficiency dramatically. Wing loading and thrust-to-weight-ratio were adjusted in several iterative steps for an adequate compromise between power and wing area. Wing aspect ratio was set as high as possible while taking the increasing stress into account that results from the high lever of the wing tip engines. Sweep angle was set according to cruise mach number after [6]. For good-tempered stall characteristics and to prevent tip stall the wing is twisted geometrically by three degrees. Considering wing sweep and twist, an optimal taper ratio was selected for best possible approximation of an elliptical lift-distribution. Dihedral angle affects the response of the aircraft whenever it is banked. A value based on historical guidelines was chosen. Table 3 contains all relevant parameters.

reference area S_W	25m^2	taper ratio λ_W	$0,54$
aspect ratio Λ_W	9	dihedral angle Γ_W	$2°$
wing span b_W	15m	mean aerodynamic chord $\bar{C}_W$	1.705m
sweep angle φ_W	$4°$	root airfoil	NACA 2414
wing twist	$3°$	tip airfoil	NACA 2410

Table 3: Wing Geometry

The wing's position with respect to the fuselage was examined by estimating *Xargo's* center of gravity (CoG). For a stable aircraft it should be located at 30% of the wing mean aerodynamic chord [6].

Because a maximum lift coefficient of $C_l = 2.5$ is to be realized, the wing integrates a shape morphing structure that is able to deflect the entire trailing downwards and therefore replacing conventional flaps as high lift system. Since there is no space for ailerons left, it is intended to use spoilers for roll control. Those are also needed for rapidly decelerating the aircraft after touchdown. Control surfaces were designed based on empirical data presented in [6].

2.1.3 Empennage

For the empennage a T-tail has been chosen. This configuration promises reduction of both horizontal and vertical stabilizer reference area by up to 5%. Due to end-plate effect, the vertical tail may be reduced in size and the horizontal tail can be designed smaller since the T-tail configuration places it away from propwash and wing wake.

The required tail area is calculated using the tail volume coefficient method for initial sizing:

$$c_{VT} = \frac{L_{VT} S_{VT}}{b_W S_W} \tag{1}$$

$$c_{HT} = \frac{L_{HT} S_{HT}}{\bar{C}_W S_W}. \tag{2}$$

Typical values for twin turboprop aircraft for vertical respectively horizontal tail volume coefficient are $c_V T = 0.08$ and $c_{HT} = 0.9$, leading to the reference areas shwon in table 4. Vertical and horizontal tail moment arm L_{VT} and L_{HT} are taken from the CAD model. Regarding

aspect ratio and taper ratio, a typical value was selected based on historical guidelines from [6].

	Vertical Tail	Horizontal Tail
reference area S	4.31m^2	4.97m^2
aspect ratio Λ	1.2	4
taper ratio	0.7	0.6
tail span b	2.3m	4.46m
sweep angle φ_W	25°	18°
airfoil	NACA 0012	NACA 0012

Table 4: Tail Geometry

According to *Raymer*, a ratio between elevator chord to horizontal tail chord of 0.36 and a ratio between rudder chord and vertical tail chord of 0.46 for general aviation aeroplanes is an adequate first guess when it comes to control surface sizing.

2.1.4 Engine Installation and Propeller Sizing

Xargo is propelled forward by four propellers, driven by an electric motor each. To satisfy performance requirements, they provide a total power of $2,000kW$. The thrust of the props is divided such that the two inner engines are solely designed and optimized for cruise flight. However, they also support the outer engines during takeoff and climb. To accomplish the maximum range of 833km, motors of 515 kW each were chosen. The wing tip engines (WTE) are responsible for assuring STOL capability by tiliting the whole assembly of motor and propeller to an angle optimized for shortest takeoff distance possible. They provide a power of $485kW$ each. To minimize the drag tradeoff during cruise, the propeller blades are able to fold flush to the engine nacelle. Figure 6 illustrates the WTE with in different blade positions.

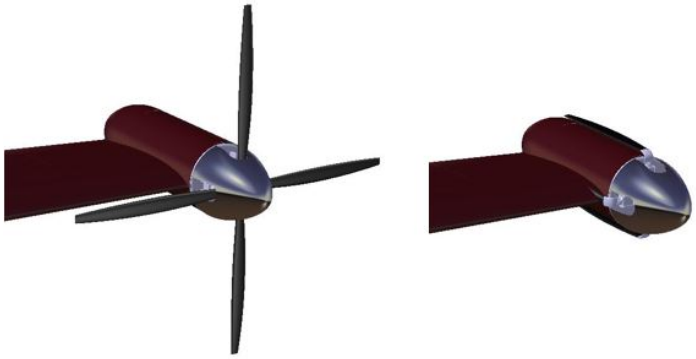

Figure 6: WTE during climb (left) and during cruise (right)

Equation () was used to calculate optimal propeller diameter as a function of engine power

$$D_{Prop} = K_p \sqrt[4]{P} \tag{3}$$

where K_p is the blade coefficient, taken from [6]. The obtained value for propeller diameter must be adjusted such that the helical tip speed does not reach sonic speed and as a consequence loses efficiency because of shock formation. This is accomplished by checking inequation ():

$$\sqrt{V^2 + (\pi n D_{Prop})^2} < 290 \frac{\mathrm{m}}{\mathrm{s}} \tag{4}$$

where a rotation rate of $n = 2,2000\mathrm{rpm}$ and a cruise speed of $V = 140 \frac{\mathrm{m}}{\mathrm{s}}$ was assumed.

2.2 Key Technologies

This chapter deals with the key technologies behind the concept. They ensure the improvement of the flight performance, with a better flow behavior, protection of the environment and work more efficiently compared to the common airplanes. The technical possibilities must be available until 2025, so the founders had to limit thereselves to the most advanced and tested technologies. For the assessment, they used the technology readiness level, or short TLR.

The Adaptive Compliant Trailing Edge [7] (TRL 8) represents a significant improvement over conventional flow control system. The shape morphing allows the airflow to follow the surface contour ideally. This can reduce fuel consumption by up to 12%. Furthermore, the control surfaces do not separate from the rest of the wing. This means that a noise reduction [8] of 30% is achieved during landing and take-off. This is applied to Xargo in the ailerons, rudder and elevator, so that the induced drag will be reduced. The high-lift-system will consist of a combination of conventional and morphing wing in order to generate the highest possible lift. This is of great importance for the STOL properties to start even on the shortest distances.

To further increase efficiency, we rely on Sharkskin technology (TRL 8) [9]. The Sharkskin consists of thousands of small-scale structures that are variable in size and shape. This structure consists of three raised ridges and can be printed in 3-D or directly scratched into the surface. They are mounted on the suction side of the wing and the upper half of the fuselage. The Sharkskin works as “high-powered, low profile vortex generator". So, this structure ensures low frictional resistance and increased the lift-to-drag ratio of the aircraft surface up to 323% compared to standard airfoils [10]. The Sharkskin Technology favors the flow behavior and can save up to 1% of the energy in flight. That means the airplane must carry less hydrogen to fly the full mission. Both technologies are already well developed and therefore realistic for implementation until 2025. They will significantly increase the efficiency of Xargo, keeping operating costs low and protecting the environment from noise and pollutant.

2.3 Mass Estimation and Center of Gravity

To obtain an adequatelly accurate estimation of mass and CoG several methods are employed. In a first step a rough estimate based on [6] is established. The design takeoff gross weight (DTGW) W_0 is added up by crew, payload, fuel and empty weight. Both crew weight and payload weight can be taken easily from the design requirements. Fuel weight and empty weights are replaced by fractions of total weight as they are dependent on DTGW and therefore must be determined in an iterative process. DTGW can finally be solved with equation

$$W_0 = \frac{W_{crew} + W_{payload}}{1 - (W_f/W_0) - (W_e/W_0)}. \tag{5}$$

Since there is little data known for hydrogen powered four engine aircraft, both empty weight fraction and fuel weight fraction were calculated using formulae for twin turboprop for a first estimation. Empty Weight fraction is given by the empirical relation

$$\frac{W_e}{W_0} = AW_0^C \tag{6}$$

which can be further reduced by 5% as *Xargo* is designed to consist of advanced composite structure. Coefficients A and C are from [6].

For fuel weight fraction mission requirements for maximum chosen range must be taken into account. The mission is approximated as a sequence of warmup and takeoff, climb, cruise and descent, second climb, cruise and descent (consisting 45 min energy reserve and additional 100 NM in case of aborted landing) and landing. For each segment, weight fractions are estimated based on historical data and *Breguet equation* is used for cruise segment. Propeller efficiency was assumed to be $\eta_P = 0.8$ and lift-to-drag ration was taken from empirical relationship between $(L/D)_{max}$ and wetted aspect ratio.

After determining thrust-to-weight ratio and wing loading a more refined sizing method was employed. Hereby, the empty weight fraction is given by

$$\frac{W_e}{W_0} = a + bW_0^{C_1} A^{C_2} \frac{hp}{W_0}^{C_3} \frac{W_0}{S}^{C_4} V_{max}^{C_5} \tag{7}$$

taking into account maximum speed V_{max}, wing loading W_0/S and power loading hp/W_0. Furthermore, fuel weight fractions are adjusted, considering mach number at initial cruise altitude and actual L/D from performance calculations. This method yields an aircraft mass of approximately 4000kg, keeping in mind that *Xargo*'s empty weight might actually be higher since it has several design features that deviate from a standard twin turboprop configuration. These are: two additional engines, use of electric motors instead of turbine engines, hydrogen fuel tank, folding mechanism between cockpit and cargo/passenger compartment, enclosed and removable cabins for payload and pilot. On the other hand fuel weight can expected to be reduced by 2/3, according to own calculations. Since both empty and fuel weight strongly depend on another, for DTGW an additional 500kg were added and required mass of hydrogen was determined from performance calcuations, assuming an aircraft total mass of $4500kg$. Empty weight was further refined using a component buildup model based on empirical formulae from both [6] and [11]. Because suggested equations by no means represent contemporary developments, adjustments are made accordingly. The equations for general aviation aircraft category are used and a weight breakdown could be examined separating structural weight, powerplant weight and fixed equipment weight. As presumed, the more refined component buildup model leads to an increased empty weight in comparison to the previously conducted mass estimation based on empirical data of twin turboprop aircraft. This would normally mean that fuel weight must be adjusted however because fuel weight was calculated with a more conservative weight than obtained by the former method, we see no need for correction in fuel weight at this point. Table 5 presents the results of the different approaches.

	Mass Estimation (Twin Turboprop)	Refined Mass Estimation (Twin Turboprop)	Component Buildup
Crew	100 kg	100 kg	-
Payload	907 kg	907 kg	-
Fuel Weight	539 kg	521 kg	-
Empty Weight	2,146 kg	2,420 kg	3,712 kg
DTGW	3,692 kg	3,948 kg	-

Table 5: Comparison of different mass estimation method results

Table 6 provides an overview of the final estimated aircraft mass, including an empty weight breakdown, crew and payload weight, fuel weight, maximum zero fuel mass (MZFM) and DTGW as well as a rough estimation of the aircrafts CoG.

	Component Mass [kg]	Component CoG [m]
Crew	100	2.8
Payload	907	6.8
Empty Weight	3,727	6.78
Structure	1,287	-
Wing	342	6.96
Horizontal Stabilizer	35	14.62
Vertical Stabilizer	34	13.98
Fuselage	620	6.8
Main Landing Gear	197	8.0
Nose Landing Gear	59	1.2
Power Plant	1,739	-
Engines	454	6.33
Fuel System	1,285	7.27
Fixed Equipments	701	-
Flight Controls	137	8.0
Hydraulic System	41	8.0
Electrical System	121	3.0
Avionics	44	2.0
Air Conditioning System	126	5.5
Furnishings	232	5.5
MZFM	4,734	6.7
Fuel Weight (H2)	111	11.7
DTGW	**4,845**	**6.81**

Table 6: Component Mass Breakdown

2.4 Propulsion Strategy

2.4.1 Propulsion System Choice

In Table 7, some supply-chain characteristics for different energy sources are listed [12]. To check them against each other the properties of a battery-system and fuel-cell-system are related to the characteristics of a conventional kerosene-system (Index: i = battery, fuel cell; k = kerosene). It shows greatly the advantages and disadvantages in point of efficiency of the different energy sources. A propulsion chain starting with batteries as energy source leads the comparison in terms of efficiency and required energy that must be stored. But what the efficiency cannot make up is that the mass specific energy of actual batteries, batteries of the next generation or in near future will not be able to store enough energy by moderate weights to be a serious alternative [13]. What seems to be a good alternative in point of mass specific density is hydrogen, which is the highest in this comparison. But hydrogen is not that convenient in handling and storing like kerosene. Also, it must be compressed or liquified, otherwise it will need up to fifty times of storage volume compared to kerosene [12]. For Xargo it was decided to consider compressed hydrogen to dodge a complex storage-management for liquified hydrogen not only on the plane, but on secluded, maybe even isolated airfields which

perhaps will not have an adequate developed infrastructure. The last row of Table 7, the relative fuel mass, figures out, that the mass of batteries will be 13 times higher compared to Kerosene. Therefore, the mass of hydrogen will split the mass for fuel to nearly a third.

	Kerosene	Battery	Hydrogen (Fuel Cell)
Total Efficiency η [%]	39	73	44
Mass Specific Energie p [Wh/kg]	11,950	500	43,000
Rel. Total Efficiency η_i/η_k	1	1.87	1.13
Rel. Energie Needed E_i/E_k	1	0.54	0.89
Rel. Mass spec. Energie e_i/e_k	1	0.042	2.51
Rel. Fuel Mass $m_{F,i}/m_{F,k}$	1	12.9	0.36

Table 7: Comparison of Energy Source Specifications

Table 8 presents mass specific densities of different energy converters to supply the propellers with shaft power. Fuel cells supple electric energy. That must be considered in this comparison and an electric motor (e-motor) must be added. To do so the reciprocals of the power densities are totaled up and inverted back. This results in a mass specific power for a fuel cell driven propeller of about 1,82 kW/kg. Until 2038 the power density is expected to be around 13 kW/kg [14]. Extrapolated to 2025 based on already proved electric engine with power densities around 5,2 kW/kg, the power density is assumed to be approximately 7,6 kW /kg in 2025. In these days values of 7,5 kW/kg are already available (e.g. EMRAX 348), but this is based on peak power what is only available for a short moment [15].

	Turbine Engine	Electric Motor	H2 Fuel Cell [16]
Mass specific Power p^* [kW/kg]	5-8	7.6	2.8 (2.1 with e-motor)
Rel. Mass spec. Power p_i^*/p_k^*	1	0.95-1.52	0.26-0.41

Table 8: Mass specific Power

The results of table 7 and table 8 combined show that a fuel cell system (fuel cell, amount of fuel and e-engine) will save mass in point of fuel but it will be heavier in point of converting energy. Overall it will be a little bit heavier (round about 1,24 times) compared to a conventional turbine and kerosene system. For Xargo we decided to go for a fuel cell system with compressed hydrogen and electric engines driving the propellers.

2.4.2 Fuel Cell

There are different kinds of fuel cells available. For the service in an aircraft some of them fit better than some others. Polymer electrolyte fuel cell (PEFC) systems for example. Table 9 shows the characteristics of a PEFC. PEFC also serves with the highest mass specific power (up to 2,8 kW/kg).

	Operating Temperature [°C]	Cell Electric Efficiency [%]	Oxidant
PEFC	80	50 to 68	Hydrogen, Oxygen (pure/air)

Table 9: Characteristics of a PEFC

Mass and Dimensions

The mass and volume power densities $P_{m,FC}$ and $P_{v,FC}$ of a PEFC can be assumed with mass

specific power density $P_{m,FC} = 2.8$kW/kg and $P_{v,FC} = 3.4kW/l$ [16]. Calculated with an installed total power of 2,000 kW that will be split into four PEFCs the mass and dimension of one fuel cell is determined to:

$$m_{FC} = 178kg$$
$$V_{FC} = 147l \approx 150l.$$

Specific fuel consumption
The specific consumption b_{H2} of a hydrogen-oxygen-fuel-cell, as the PEFC, is derived by the amount (mole) of hydrogen that is necessary for an amount of electrical energy output. This is estimated with 237 kJ/mol [17]. Converting it by using the molar mass of a H2 molecule the reciprocal and specific consumption is given to $b_{H2} = 0.00851g/kJ$. It is important to notice, that this is the consumption of hydrogen only. How much oxygen will be used is estimated by a look on the chemical equation of the fuel cell process [18]:

$$\mathrm{H_2} + \frac{1}{2}\,\mathrm{O_2} \longrightarrow \mathrm{H_2O}. \tag{8}$$

This equation figures out, that for one H2 molecule there is a half O2 molecule needed, so that the demand of oxygen is half of the hydrogen consumption, $b_{O2} = 0.00425$g/(kWs). It is intentionally spoken of a demand of oxygen, because the requirement can be supplied by the airflow around the aircraft.

2.4.3 Storage System

Estimation of the required amount of hydrogen
The amount of hydrogen is estimated by using the results of the performance calculation as well as using handbook methods. The performance data helps to calculate energy required of each section. table 10 gives an overview of the energy consumption of each mission section.

Normal Mission				
Takeoff	Climb	Cruise	Descent and Loiter	Approach
18,267 kJ	1,630,532 kJ	4,664,529 kJ	1,087,266 kJ	658 kJ
Reserve Mission				
Extra Fuel (45min)	Climb	Divert	Descent and Loiter	Approach
2,540,183 kJ	1,630,532 kJ	268,802 kJ	1,087,266 kJ	658 kJ
Sum: 12,928,675 kJ				

Table 10: Energy Consumption

Storage Seizing
To determine the needed storage capacity the calculated amount of energy (12928675 kJ) is multiplied with the specific consumption (0,008505 g/kJ) of the fuel cell and divided with the density of compressed hydrogen of 40 kg/m3. As Result there is a storage capacity of 2,75 m3 required. For an optimized stress distribution in the storage structure, the storage geometry is chosen as circular cylinder with half spherical caps. The capacity of the pressure tank can then be calculated by the volume of a sphere and a circular cylinder. To reduce weight, the storage will be made from CFRP. For the following estimation the next assumptions are made [19]:

- Pressure only results in a force parallel to the fiber direction,
- breaking strength is approximated by $R_{II} = R_{II,F} \cdot \Phi_F$,

- fiber volume fraction Φ_F is set to 60% and
- allowed stress is half of the breaking strength, due to safety considerations.

For a rough weight estimation of the hydrogen storage, its wall thickness is calculated by the following equation:

$$t = \frac{r_i \cdot p}{\sigma} \tag{9}$$

wherein r_i is the inner radius, p is the pressure and σ is the allowed stress. With the specifications of carbon fibers ($\Phi_F = 0,6$, $R_{II,F} = 3900\text{N/mm}^2$, $R_{II} = 2340\text{N/mm}^2$) and the assumptions above the allowed stress is calculated to 1170N/mm^2. The density of the carbon fiber and matrix material is assumed to $\rho_F = 1,800\text{kg/m}^3$ and $\rho_M = 1,200\text{kg/m}^3$. For a pressurized cylindric storage the storing capacity grows exponentially with increasing diameter compared to increasing linear with greater length. Hence, it is more efficient to choose one big tank than a couple of small ones from a geometric point of view. But it must be considered that the weight of the storage also grows exponentially. In this regard, it is more beneficial to split the needed storage capacity into a couple of smaller storages. For Xargo we splitted the required storing capacity into five tanks. One big storage (capacity $\approx 1,64\text{m}^3$) in the rear of the fuselage and four smaller tanks (capacity $\approx 0,27\text{m}^3$ each. Total weight of the storage system is added up to 570 kg.

3 Flight Mission Analysis

3.1 Operation and Logistics

For multimodal operation an interior change has to occur switching from an only passenger to an only cargo configuration. The passenger cabin provides a door which can be closed and locked for the time it is not needed and therefore stands on the airport terrain. The cabin consists of 2 layers. The inner one holds the screens whereas the outer one provides protection from weather circumstances. The cabin is made of CFRP to provide high stability and weight advantages. The outer layer is covert with a water proof coating. If attempted to be stolen or broken into, a 2025 state of the art alarm system is included within the walls. Figure 7 represents the design of the cargo wagon. It is carried by the same base design as is the passengers cabin. 2000 pounds are supposed to be carried. The estimation of the cargo box size, the density of water is the baseline. A cube with the side lengths of 39.4 inch (1 m) was chosen to fit the cargo goal. For easier loading, the back wall of the box can be detached by lifting it. A plug-in socket provides the necessary stability. The cargo box is made of CFRP. Cargo can be put in the box or, if not fitted, bonded in front and/or behind the box with tension straps. The cargo floor provides 4 eyebolts on each side of the cargo box in order to prevent loose luggage to shift.

Within the floor, a 2025 state of the art GPS controll- unit and electronical rotors will provide an autonomous rolling out of the fuselage and to a designated position at the gate of the designated airport. There, it can be un- and reloaded by the respected logistic company. The GPS coordinates for parking should be callibrated into the system before the flight for the respected airport. This requires an available space (hence coordinates) for parking of the sytem. Furthermore, optical sensors prevent the collition of the system with an other obstacle. The command of starting the process of rolling out, is starting 5 minutes after the plane reached the designated gate. In case of a gate change, the operating company will receive a message by the system, asking for recallibrating the parking position of the box.

Figure 7: Cargo Wagon

If failed to react, the aircraft will not open automatically and hence, the box will not roll out. Manually, the aircraft can be opened by an authority for the process to start. It is also possible for the operating airline to start unrolling via remote control. For stearing back in, the cargo wagon automatically drives in front of the fuselage opening. Optical sensors allow the cargo system to roll into the fuselage without collision. This process can be started from the operating airline via remote control.

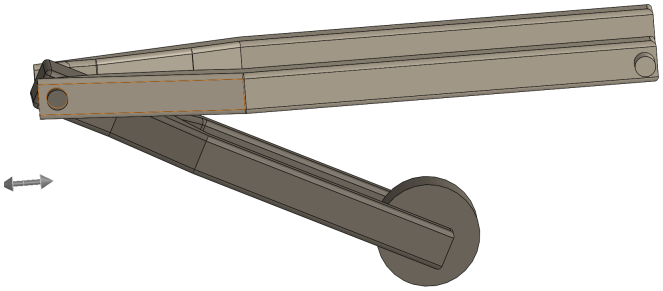

Figure 8: Folding Mechanism

Since it could be expected that the aircraft needs to land on small airports possibly providing a rough or non-paved road, the wheels are made of rubber. The structure is provided with suspension. The rest of the leg is made of aluminium. The legs are composed of generally three parts. Similar to a human leg, its mid-joint enables the lower leg to move forward when the wheels are detouching the rails of the fuselage. Electrical motors includin a control unit drive the wheels of the legs. Rolling back into the fuselage, elecrical motors on the upper and mid-joint, lift the device to its original position. The autonomous system is expected to fit the requirement to switch from only passengers to an only cargo flight.

3.2 Mission Plan

With our aircraft design we offer the possibility to fulfill any kind of task in City areas in the outback, with passengers or cargo. The protection of the environment and the handling with a minimum of ground infrastructure at airports is very important for the project. This is realized by the newest technologies for noise reduction, exhaust pollution, autonomous loading and unloading as well as the possibility of unmanned flight control. The modular design of Xargo ensures a rapid ground handling of passengers and cargo. Therefore, the

turnaround-time is at a minimum in order to fly as many missions as possible. After the boarding of the passengers or loading of the cargo, as described in the section Operation and Logistic, the aircraft is ready for departure and maneuvers with the electrically driven landing gear to the runway. The airplane accelerates with the engines for cruise and the engines at the wingtip pitched up on a route of 97m and finally lifts off. This is followed by a climb phase with all engines, up to 10000 ft at velocity CAS (Calibrated airspeed) of 250 kts and a climb rate of about 10 m/s. After crossing the restricted airspace, it climbs with Cruise Mach Number of 0.45. At the altitude of 25000 ft the cruising altitude has been reached. In this part, the tiltable engines are retracted at the end of the wing. Only the cruise engines continue to run in their optimum range. This significantly reduces energy consumption, noise emissions and aerodynamic drag. The descent flight path is divided in two sections. Up to 10000 ft with Cruise Mach Number of 0.45 and below limited again with 250 kts. The 24 hours mission plan is separated in two sections. In both parts it is flown with a cruise speed of about 140 m/s over a distance of 120 nmi (see figure 9). Therefore, it takes 26.5 minutes for one flight. In the first part the plane transports passengers in the passenger configuration and at first with the single pilot cockpit. This going to be changed, after unmanned flights with passengers are allowed. Here every turnaround takes 45 minutes. Over the 12 hours of the first section, it is possible to cover ten flights. After the 12 hours the plane is going to be configurated in to the cargo version. So the cockpit is unmanned and the fuselage now contains the cargo. This section is set to six hours with the same speed, distance and time as the passenger flights. The turnaround is now 30 minutes and done by the automatic loading system of the airplane. As shown in Figure 9 Xargo is able to fly 6 missions.

	Cargo	PAX
$V_C := 140\ \frac{m}{s}$	$t_{turnaroundCargo} := 30\ min$	$t_{turnaroundPAX} := 45\ min$
$d := 120\ nmi$	$t_{missionCargo} := t + t_{turnaroundCargo}$	$t_{missionPAX} := t + t_{turnaroundPAX}$
$t := \frac{d}{V_C} = 26.457\ min$	$n_{flightsCargo} := \frac{(6\ hr)}{t_{missionCargo}} = 6.377$	$n_{flightsPAX} := \frac{(12\ hr)}{t_{missionPAX}} = 10.076$

Figure 9: Number of Flights

3.3 Unmanned Operation

One of the most interesting task-position of the design challenge is the autonomous flight. It will perform cargo missions without a pilot and in a computer-controlled or remote-controlled aircraft. Currently, modern aircraft have many assistant systems. Thanks to these systems, pilots are able to achieve safer flight, especially when landing and taking off. In addition, the autopilot is another system that has been used for many years. The use of all these systems together allows the aircraft to perform most of their missions autonomously. Xargo is a fully autonomous aircraft and has the ability to be remotely commanded during take-off and landing, which is one of the most critical phases of flight. In this way, dangerous situations that can be experienced, can be eliminated. Autonomous flight consists of two different perspectives. The first is the devices that are on board and second the infrastructure in the airport. The aircraft has separate systems for each flight phase. These systems work in symbiosis with another. Autonomous flight has the ability to fly and route in the same way as previously scheduled, as well as the ability to detect and react to commands given by air traffic control. In this way, it is dynamically integrated into air traffic. Secondly, modern

airports have many infrastructure as ILS. It does not require any additional system for the operation of the aircraft in such modern and multi-device airports. But due to the short-distance-aircraft, our aircraft has also the ability to operate in smaller airports. In order to have this capability, it will be cheaper (instead of the expensive ILS system) and expected to be developed in the next 6 years Satellite Landing System GBAS.

The following list points out both benefits and challenges that have to be faced with regards to autonomous flight.

Benefits [20]:

- The unpressurized cabin can be used,
- Less danger, nobody will die in the event of an accident,
- No pilot costs,
- Less fuel,
- Less DOC,
- The accident due to the pilots can be avoided with the help of autonomous aircraft technology,
- Flexible crew planning,
- Ruduce ecological footprint and noise,
- Create new jobs such as: UAS engineers, software developers, manufactures, maintainers etc.

Disadvantages:

- If something goes wrong, the autonomous aircraft can not work spontaneously,
- Critical instruments can fail,
- The passengers do not trust, that means less ticket sales.

In order to make autonomous flight more comprehensible, workflow diagrams were prepared to show which systems work in coordination with each other for different phases of flight. Along with the systems already in modern aircraft, some systems have been added to allow autonomous flight.

3.3.1 Taxi Way

The systems that will be used for Taxi are activated after boarding the passengers or loading the cargo. The Taxi-Way checklist is checked and all systems have status “operate”. Request for Taxi has been taken by Airport Ground Control (via Voice Command System). Then, the lane assist system and the radar control continuously until the runway. The camera and radar also control around of the aircraft. Any dangerous approach is detected beforehand and the aircraft stops.

3.3.2 Ground Run

The plane stops when the taxi is complete and the plane reaches the runway. Permission is taken for departure (via Voice Command System). The take-off checklist is checked and all necessary controls are provided. Once the takeoff permit is obtained, the aircraft accelerates

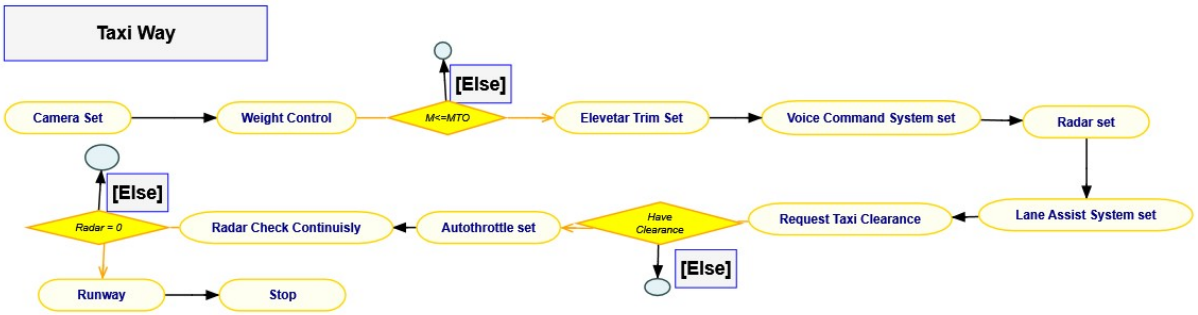

Figure 10: Taxi Way

on the runway. The radar and camera continuously monitor the environment. The sensors in the engines continuously send information to the control computer of the aircraft against any engine failure. In case of engine failure, the aircraft follows the procedure as previously programmed in parallel with the information provided by the speed sensor. After take off, it continues to climb to a altitude of 1500 ft, thus ending the take-off phase.

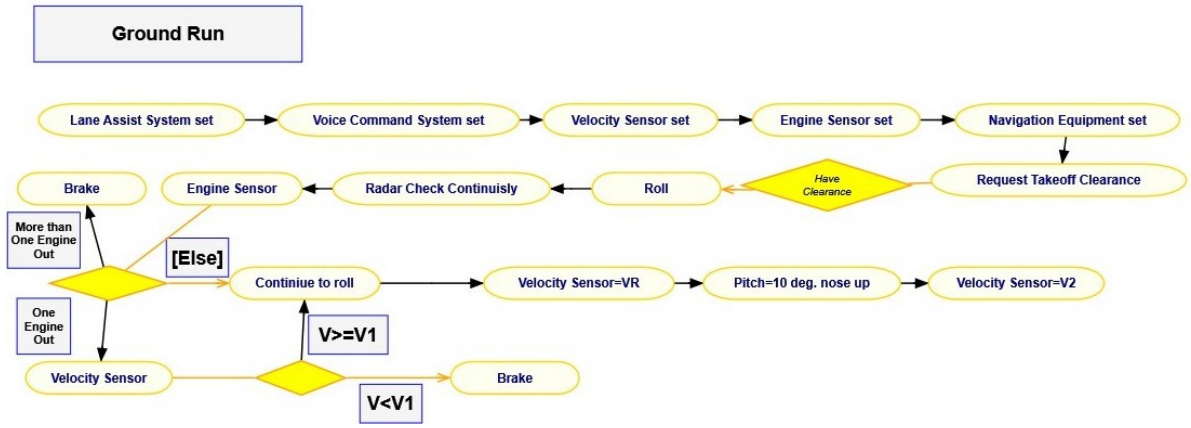

Figure 11: Ground Run

3.3.3 Climb

During climb, the aircraft is in communication with air traffic control. It is capable of reacting immediately to incoming commands. Information from the flight path angle sensor is continuously checked. Furthermore, the speed of the aircraft is kept constant at 250 kts until it reaches 10000 ft. The airplane continues to climb in parallel with the pre-programmed information from the air traffic control. When it reaches ICA, the climb phase ends and the cruise phase begins.

3.3.4 Cruise

Once the cruise altitude has been reached, the aircraft fix the aircraft speed at 0.45 Mach and continuously controls it with velocity sensors. The cabin pressure is continuously controlled and acts the aircraft as pre-programmed if a low cabin pressure is detected. Radar check the environment continuously in order to detect dangerous approaches in advance. Thanks to the navigation system, the aircraft moves towards its destination.

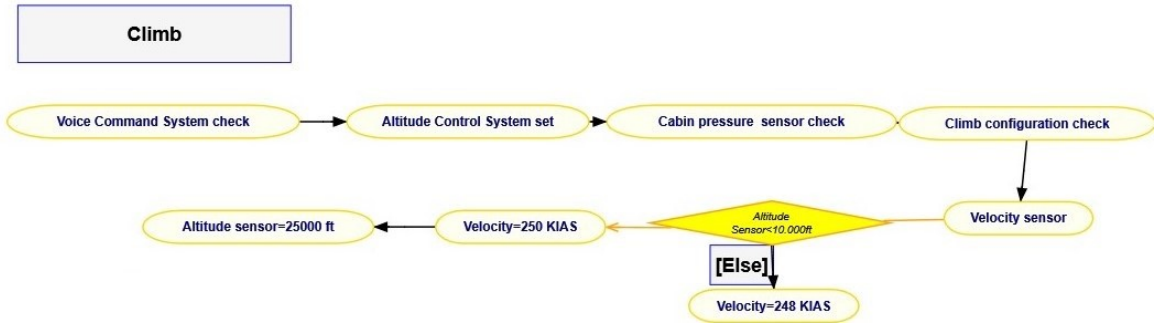

Figure 12: Climb

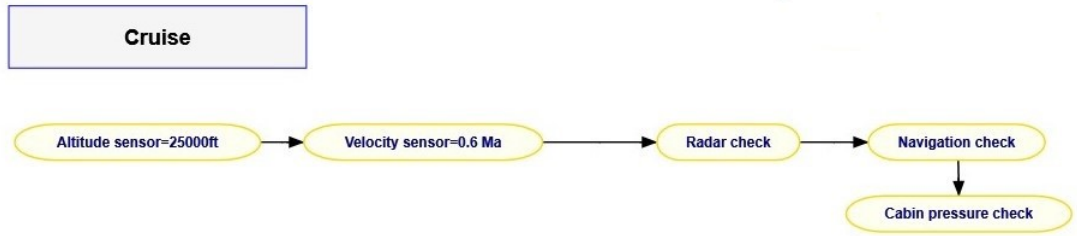

Figure 13: Cruise

3.3.5 Descent

Engines for descent produce as little thrust as possible. The descent angle and the altitude sensor are continuously checked. The cabin pressure is continuously controlled and, if a negative condition occurs, it acts as pre-programmed.

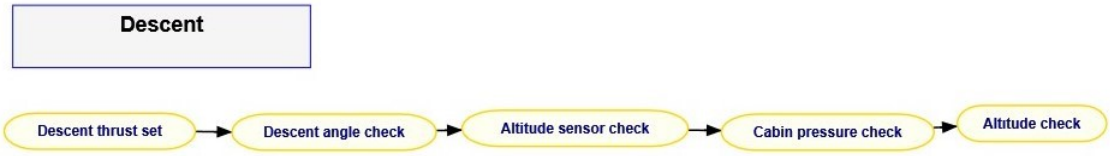

Figure 14: Descent

3.3.6 Landing

Approach angle is continuously controlled before landing.The aircraft makes contact with Air traffic control and necessary permissions are taken for landing. The landing checklist is checked and the landing configuration is set. After touch down aircraft brakes on the runway correctly and smoothly by the lane assist system. Then it makes contact with the Airport Ground Control and leaves the runway in the appropriate taxi way.

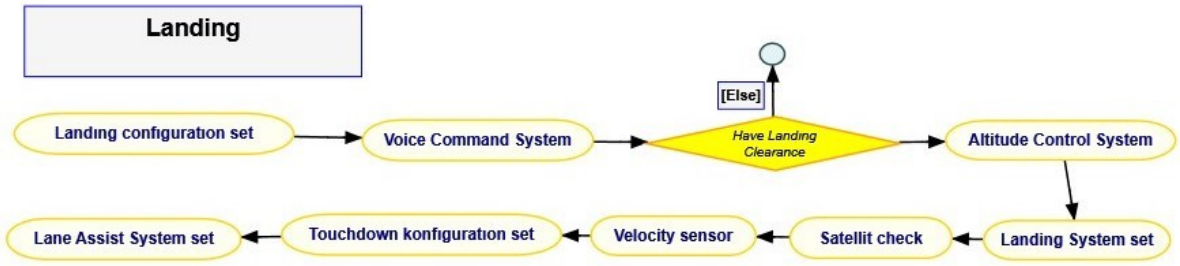

Figure 15: Landing

4 Performance Data

4.1 Takeoff

The takeoff distance is limited to at most 1,000 ft taking 35 ft of obstacle clearance into account. To reach the closest value to the 250 ft takeoff target a low wing loading along with high maximum lift coefficient is favourable. However, low wing loading negatively affects climb and cruise performances. The maximum lift coefficient is not expected to exceed values of 2.5 without a sophisticated high lift system, containg multiple slotted flaps. For these reasons, we rather have focussed on increasing the thrust-to-weight ratio, which is the third variable that affects takeoff distance. This mainly allows to simplify the wing geometry und decrease the otherwise needed large reference area and therefore increases lift-to-drag-ratio towards its optimal value. By varying the thrust vector of the WTE a vertical force component contributes to the lift and this way decreases stall speed and takeoff speed, respectively. During flare the WTE were determined to have a larger thrust angle than during ground run.

The total distance is determined by two segments: the ground run and the flare [21]

4.1.1 Ground Run

Assumptions [22]:

- aircraft is considered as a mass point,
- smaller angle of attack: $\alpha << 1$,
- no inclination of the runway,
- no wind influence.

First, the balance of forces is determined:

$$m_{TO}\dot{V} = T_1 + T_2 \cos\sigma - \mu_R m_{TO} g - (D_R - \mu_R L_R) + \mu_R T_2 \sin\sigma \tag{10}$$

where L_R is the lift in Newton on the aircraft, m_{TO} is the mass in kg of the aircraft, g is the standard gravity of $9.81 m/s^2$, V is the velocity in m/s,T_1 is the thrust in Newton from inside Motors, T_2 is the thrust in Newton from motors located on the wing ends,σ is the motor thrust angle in $^c irc$, μ_R is the coefficient of kinetic friction, where D_R is the drag in Newton on the aircraft.

$$\dot{V} = \frac{dV}{dt}\frac{dx}{dx} = V\frac{dV}{dx} \tag{11}$$

The distance for Ground Run is determined from these (1),(2) equations.

$$s_{Gr} = \int_0^{V_{LOF}} \frac{m_{TO} V}{T_1 + T_2 \cos\sigma - \mu_R m_{TO} g - (D_R - \mu_R L_R) + \mu_R T_2 \sin\sigma} dV \tag{12}$$

where V_{LOF} is the velocity at liftoff. From equation (3), distance for ground run is calculated:

$$s_{Gr} = 54\text{m}. \tag{13}$$

4.1.2 Flare

Assumptions [22]:

- aircraft is considered as a mass point,
- trajectory is approximately a circular arc,
- constant liftoff velocity V_{LOF},
- smaller flight path angle $\gamma << 1$,
- no wind influence.

First, the balance of forces is determined [23]:

$$0 = T - D - m_{TO} g \sin\gamma \tag{14}$$

$$m_{TO} \frac{V^2}{r} = L - m_{TO} g \cos\gamma \tag{15}$$

The radius is determined from these equations:

$$r = \frac{V^2}{g(n - \cos\gamma)} \tag{16}$$

where r is the radius in meter of circular arc, n is the load factor. Distance for Flare can be calculated with:

$$s_F = r \sin\gamma = 118\text{m}. \tag{17}$$

$$s_{Total} = 172\text{m}. \tag{18}$$

4.2 Climb

Climbing starts at 1500 ft after take-off and continues up to the ICA 25000 ft. For a better take-off performance, the outboards motors are set back to 0 degrees during climb. Calculation of climb performance and climb time are done in 3 steps. In typical for commercial aircraft flight missions, the climb phase usually has following procedure:

1. Climbing from 1,500 ft to 10,000 ft at a constant velocity CAS (Calibrated airspeed) of 250 kts,
2. Climb with Ma_{Cruise} to the initial cruise altitude (ICA).

Balance of forces:

$$m_{TO} \dot{V} = T \cos(\alpha + \sigma) - D - m_{TO} g \sin\gamma \tag{19}$$

$$m_{TO} \dot{\gamma} V = T \sin(\alpha + \sigma) + L - m_{TO} g \cos\gamma \tag{20}$$

where $\dot{\gamma}$ is the angular velocity in s^{-1}.

Assumptions [22]:

- flight path angle $\gamma = const$,
- smaller flight path angle $\gamma << 1$,
- constant velocity V,
- thrust angle $\sigma = 0$,
- smaller angle of attack $\alpha << 1$.

Flight path angle is determined by equations (10) and (11):

$$\sin\gamma = \frac{T}{m_{TO}g} - \frac{\cos\gamma}{E} \tag{21}$$

where E is the Lift-to-drag ratio. With small flight path angle $\gamma << 1$:

$$\sin\gamma \approx \gamma, \quad \cos\gamma \approx 1 \tag{22}$$

it follows:

$$\gamma = \frac{T}{m_{TO}g} - \frac{1}{E}. \tag{23}$$

Results may be taken from Appendix.

4.3 Cruise

Initial Cruise Altitude (ICA): Requirement of a climb rate of 500 ft / min at max. Ma Number When reaching the Cruise altitude ICA, the aircraft must be at the maximum Climb Performance the engines still have a sufficient rate of climb. Typical climbing speeds are 500 ft / min [22]. Climbing speed is determined by equations (12) and (14): $\boldsymbol{\dot{H} = 28.4\frac{\mathrm{m}}{\mathrm{s}}}$.

4.4 Descent

Descent with these processes [21]:

- H_{Cruise} – 10,000 ft: Descent with max. Cruise Velocity,
- 10,000 ft: Velcity reduction $V_{Descent}(CAS) = 250$kts,
- 10,000 ft – 1,500ft: Descent with $V_{Descent}(CAS) = 250$kts.

Assumptions [22]:

- smaller Flight Path Angle $\gamma << 1$,
- the engine power is redeuced as much as possible during descent,
- thrust angle $\sigma = 0$,
- smaller angle of attack $\alpha << 1$,
- constant Velocity,
- Flight Path Angle $\gamma = const$.

The balance of forces is determined [23]:

$$0 = T\cos\alpha - D - m_{TO}g\sin\gamma \tag{24}$$

$$0 = T\sin\alpha + L - m_{TO}g\sin\gamma \tag{25}$$

Descent Velocity w can be found with help of equations (15) and (16):

$$w = -V\sin\gamma. \tag{26}$$

Altitude[ft]	25000,00	24000,00	20000,00	17000,00	10000,00	5000,00	1500,00
TAS [m/s]	140,00	139,90	142,20	144,16	148,04	138,62	131,54
Descent velocity [m/s]	9,29	9,33	10,67	11,83	15,13	14,45	13,71
Descent velocity average [m/s]		9,31	10,00	11,25	13,48	14,79	14,08
ΔH [m]		304,80	1219,20	914,40	2133,60	1524,00	1066,80
t[s]		32,74	121,90	81,25	158,28	103,07	75,78
Σt[s]				573,03			

Table 11: Time for Descent

4.5 Landing

To fulfill the task of landing distance have thrust the outer motors against the direction of the weight. So has a thrust angle 90 degrees. This achieves a small landing distance. The total distance is determined by 2 phases [21]: the flare and the breaking.

4.5.1 Flare

$$m_L\dot{V}_L = -D - m_L g\sin\gamma - T\sin\gamma \tag{27}$$

$$0 = L - m_L g\cos\gamma + T\cos\gamma \tag{28}$$

Assumptions [22]:

- aircraft is considered as a mass point,
- flight path angle $\gamma = const$,
- smaller angle of attack: $\alpha << 1$,
- no wind influence,
- constant deceleration $\dot{V}_L$,
- smaller flight path angle $\gamma << 1$.

Equations (27) and (28) determine the Flare distance.

$$s_F = 107\text{m}$$

4.5.2 Breaking

$$m_L \dot{V}_L = T - D_R - \mu_B N_z \tag{29}$$
$$0 = -m_L g + N_z \tag{30}$$

Assumptions [22]:

- aircraft is considered as a mass point,
- no thrust in flight direction (perhaps reverse thrust),
- no Lift (by use of spoilers),
- no inclination of the runway,
- no wind influence.

$$s_{Br} = 172\text{m}$$
$$s_{Total} = 279\text{m}$$

5 Evaluation

5.1 Costs

To estimate the life cycle costs of Xargo were handbook methods used. To determine RDT&E (research, development, testing and evaluation) and production cost the modified DAPCA IV (development and procurement costs of aircraft model) cost model were used [6]. There were 20% added due to more operational testing of the unconventional propulsion system and manufacturing of complex composite structures. The purchase cost of Xargo includes 10% surcharge and is about $ 4.829.041 and so 12 % more expensive as a Pilatus PC 12 [24]. But as Figure 16 shows Xargo will save operational costs such as fuel [25], [26]. The direct operating costs were calculated by the AEA model (Association of European Airlines) [27].

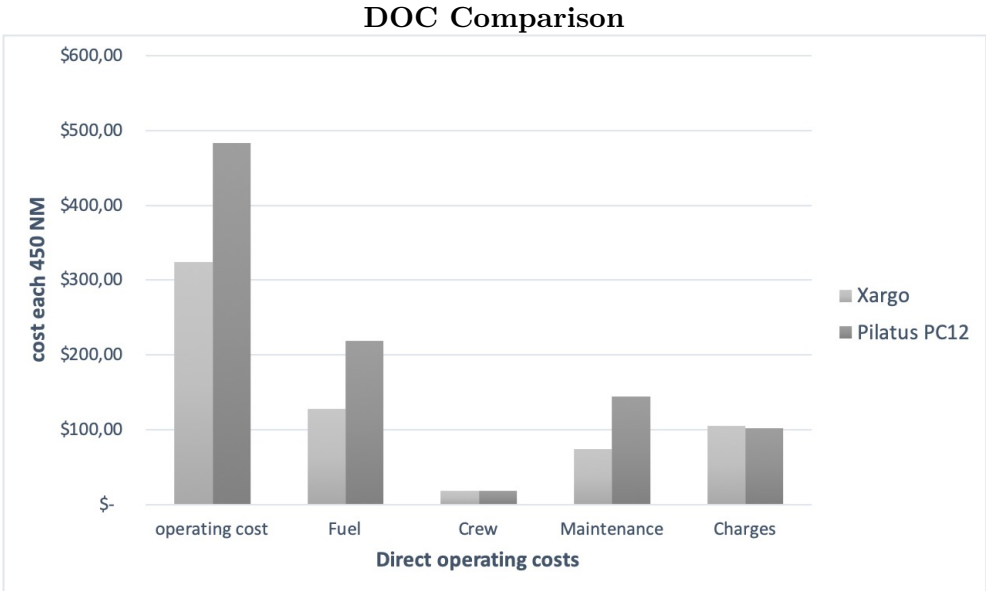

Figure 16: Comparison of DOCs: Xargo vs. Pilatus PC12

5.2 Risk and Failure Assessment

Along the way of designing Xargo, certain design features have been implemented which prevent failure or damage that could potentionally affect the passenger's safety or the aircraft's structural integrity.

- **Swivel Mechanism**: During turnaround the nose of Xargo will be swiveld sideways to open the fuselage for loading or unloading of the payload module. To counteract any instability or damage to the joint, a lever extends to the ground.
- convertable between passenger and cargo configuration in less than one hour,
- **Foldable Propeller Blades**: While retracting the propellers of the WTE they must be positioned in a way that they do not clash with the wing itself. To ensure so, there is a positioning sensor considered which knows exactly the position of blade and will force the propeller to rotate into the necessary position to be folded.
- **Hydrogen**: Hydrogen is highly flammable and, when combined with oxygen in a certain ratio (for example the oxygen in the air), a highly explosive fuel. Due to that fact, there must be taken measures to ensure that there is no hydrogen leaking. A 100% guaranty is barely viable, which is why the entire fuel system has to be covered with an additional layer. Underneath that layer will be no ignition power big enough to possibly ignite any released H2. The same safety measure must be ensured at the ground fuel supply system. Another point of concern was the positioning of the hydrogen tanks. They are intentionally not placed near the bottom of the fuselage to consider a balked landing or ditching.
- **WTE Failure**: a WTE failure happening during flare or approach will be one of the most crucial safety risks around the key features of Xargo. There will be just a short time to counteract the sudden roll- and gear moment that Xargo will experience in that kind of situation. This is as a great challenge for the flying-computers, engine controlls as well as for the position sensors to react quick enough with reducing the power of the operating WTE.

6 Conclusion and Outlook

Xargo fulfils all requirements were set. The modular structure allows a quick conversion between a passenger setup to a frighter. Table 12 summarizes how Xargo complies with the requirements.

	Threshold	Goal	Xargo	Design Feature
passengers	9	-	9	-
payload	2,000 lbs	-	2,000 lbs	-
conversion time between passenger and freight mission	60 min	-	60 min	swiveling nose section and modular cabin and cockpit design
maximum range (no reserves)	200 NM	500 NM	450 NM	compressed H2
divert range	50 NM	100 NM	100 NM	-
takeoff and landing distance (35 ft obstacle clearance)	1000 ft	250 ft	463 ft / 915 ft (mean sea level, standard temp.)	tiltable WTE
acoustic level	80 dB(A)	65 dB(A)	80 dB(A)	-
DOC	-	0	0.72 $/NM/PAX	fuel cell powered and electrically driven engines
turnarounds (passenger mission)	-	-	10	-
turnarounds (cargo mission)	-	-	6	-

Table 12: Compliance with Requirements

Although Xargo is already a well-conceived concept, there still is room for improvement and further adjustments.

Turnaround time can easily be reduced by using more than one module (passenger cabin or cargo platform). While one module is flying with Xargo to the destination, two others could be dispatched at the airfields.

There are some potentials for Xargo 2nd generation to increase efficiency. The hydrogen storage in the back of Xargo could be conducted as module as well, so there would no unnecessary storage weight (364 kg) that must be carried through flight.

Another advancement can be done to optimize the propeller folding geometry. During cruise the propeller could be folding in a special way, so that they are extending the wingtip to create the effect as a winglet. This will increase aerodynamic efficiency of the wing and reduce required fuel.

Another way to lower fuel costs is possible, if an additional water storage will take place in Xargo. The water which is produces by the fuel cells during climb and cruise could be stored. During descent when potential energy is transferred to kinetic energy, some of this transfer could be used to split the stored water back into fuel (hydrogen) and oxygen by one fuel cell.

References

[1] U.S. Department of Transportation. *Essential Air Service*. 2017. URL: https://www.transportation.gov/policy/aviation-policy/small-community-rural-air-service/essential-air-service (visited on 06/23/2019).

[2] D. Wolf. *Commuter Airline Perspective*. 2016. URL: http://www.nianet.org/ODM/ODM%20Tuesday%20presentations%20Final/13%20Wolf%20FINAL%20Cape%20Air%20NASA%20ODM%20Conference%20deck%20v7MAR16.pdf (visited on 06/23/2019).

[3] G.V. Mikic A.M. Stoll. "Design Studies of Thin-Haul Commuter Aircraft with Distributed Electric Propulsion". In: *AIAA 2016-3765* 16th AIAA Aviation Technology, Integration and Operations Conference (June 2016).

[4] VDMA. *Photonic Industry Report 2017*. 2017. URL: https://photonik.vdma.org/documents/433966/18769673/VDMA_Photonik-Branchenreport-2017_final_1499938258930.pdf/131364ff-5093-450c-b964-0d8a1820923c (visited on 06/26/2019).

[5] statista.com. *worldwide spending display panels by application 2016-2023*. 2019. URL: https://www.statista.com/statistics/987337/worldwide-spending-share-on-display-panels-by-application/ (visited on 06/26/2019).

[6] Daniel P. Raymer. *Aircraft Design: A Conceptual Approach*. Virginia: American Institute of Aeronautics and Astronautics, 2006.

[7] FlexSys Inc/2205. *FlexFoil^{TM} Compliant Control Surfaces*. 2019. URL: https://www.flxsys.com/flexfoil (visited on 06/10/2019).

[8] NASA Armstrong Flight Research Center Jelisa Beaty. *Hear This: 30 Percent Less Noise*. 2017. URL: https://www.nasa.gov/centers/armstrong/%20feature/ACTE_30_percent_less_noise.html (visited on 06/10/2019).

[9] Rebekah Andrews. *Shark skin study promises lift in airplane and turbine design*. 2018. URL: https://newatlas.com/shark-skin-aerodynamics/53295/ (visited on 06/20/2019).

[10] JP Casey. *Sharkskin design improves aircraft aerodynamics*. 2018. URL: https://www.aerospace-technology.com/news/sharkskin-design-improves-aircraft-aerodynamics/ (visited on 06/20/2019).

[11] J. Roskam. *Airplane Design, Part V: Component Weight Estimation*. Kansas: Roskam Aviation and Engineering Corporation, 1989.

[12] Martin Hepperle. *Electric Flight - Potential and limitations*. 2012. URL: https://elib.dlr.de/78726/ (visited on 06/28/2019).

[13] Heinrich Lindner. "Interview mit Prof. Dr. Martin Winter". In: *Auto Motor und Sport 2019* 2nd Auto Motor und Sport, Was ist die perfekte Zelle (Jan. 2019).

[14] Ravi Rajamani. *Electric Flight Technology: The Unfolding of a New Future*. Pennsylvania: SAE International, 2018.

[15] EMRAX. *Technical Data EMRAX 348*. 2016. URL: https://emrax.com/wp-content/uploads/2017/01/emrax_348_technical_data_4.5.pdf (visited on 06/30/2019).

[16] Jens Mitzel. *Wasserstoff und Brennstoffzellen*. 2016. URL: https://www.dlr.de/tt/Portaldata/41/Resources/dokumente/institut/elchemenergietechnik/BWK_05_2016_Wasserstoff.pdf (visited on 06/27/2019).

[17] Peter Kurzweil. *Brennstoffzellentechnik: Grundlagen, Komponenten, Systeme, Anwendungen*. Wiesbaden: Vieweg Verlag, 2003.

[18] Sven Geitmann. *Wasserstoff & Brennstoffzellen*. Norderstedt: Hydrogeit Verlag, 2004.

[19] Prof. Klaus Wolf. "Composite Aerospace Structures". In: *Script* (2017).

[20] J. Grundlach. *Civil and Commercial Unmanned Aircraft Systems*. Virginia: American Institute of Aeronautics and Astronautics, 2016.

[21] P. Horst C.-C. Rossow K. Wolf. *Handbuch der Luftfahrzeugtechnik*. Munich: Hanser Verlag, 2014.

[22] Prof. Wolf. "Einführung in die Flugmechanik". In: *Vorlesungsskript WS 18/19 TU Dresden* ().

[23] Prof. Wolf. "Luftfahrzeugauslegung". In: *Vorlesungsskript WS 18/19 TU Dresden* ().

[24] U.S. Department of Transportation. *Aerosieger*. 2015. URL: https://www.aerosieger.de/news/6347/pilatus-bringt-pc-12-ng-mit-gesteigerten-leistungsdaten.html/ (visited on 06/28/2019).

[25] POPA. *Pilatus costs*. 2016. URL: https://pilatusowners.org/wp-content/uploads/2016/02/How-Much-Does-it-Cost-to-Operate-a-PC-12-Jan-2016.pdf (visited on 06/23/2019).

[26] Bay Lukas; Palm Regine. "Die Zukunft kommt aus Wuppertal". In: *Handelsblatt* - (June 2016).

[27] Prof. Wolf. "Luftfahrzeugauslegung". In: *Vorlesungsskript TU Dresden* (2012).

A Appendix

A.1 All Engines Operative

1) Climbing from 1500 ft to 10000 ft at a constant velocity CAS (Calibrated airspeed) of 250 kts

Altitude/ft	1500		5000	10000	
TAS/(m/s)	131,5		138,6	149,7	
T,climb/kN	8,923		8,567	8,069	
$\gamma(\dot{V})$/rad	0,084		0,076	0,066	
$\dot{H}$/(m/s)	10,131		9,62	8,8	
ΔH/m		1067	1524		
$\dot{H}$,average/(m/s)		9,87	9,2		
t/s		108	166		
Σt			274		

Table 13: Climb from 1,500 ft to 10,000 ft (all engines operable)

2) Climb with Ma_{Cruise} to the initial cruise altitude ICA

Altitude/ft	10000		17000	20000	
TAS/(m/s)	148,037		144,16	142,2	
Ma	0,45		0,45	0,45	
T,climb/kN	11,18		11,77	12,07	
$\gamma(\dot{V})$/rad	0,133		0,166	0,18	
$\dot{H}$/(m/s)	17,67		21,427	22,83	
ΔH/m		2134	914		
$\dot{H}$,mittel/(m/s)		19,548	22,128		
t/s		109	41		
Σt			150		

Table 14: Climb from 10,000 ft to 20,000 ft (all engines operable)

Altitude/ft	20000		24000	25000	
TAS/(m/s)	142,2		139,9	140	
Ma	0,45		0,45	0,45	
T,climb/kN	12,07		12,46	12,53	
$\gamma(\dot{V})$/rad	0,18		0,196	0,2	
$\dot{H}$/(m/s)	22,83		24,419	24,75	
ΔH/m		1219	304,8		
$\dot{H}$,average/(m/s)		23,624	24,585		
t/s		51,6	12,4		
Σt			64		

Table 15: Climb from 20,000 ft to 25,000 ft (all engines operable)

A.1 One Engine Inoperative

Altitude/ft	1500		5000		10000	
TAS/(m/s)	131,5		138,6		149,7	
T,climb/kN	8,48		8,142		7,668	
$\gamma(\dot{V})$/rad	0,074		0,067		0,057	
$\dot{H}$/(m/s)	9		8,484		7,661	
ΔH/m		1067		1524		
$\dot{H}$,average/(m/s)		8,742		8,072		
t/s		122		188		
Σt			310			

Table 16: Climb from 1,500 ft to 10,000 ft (one engine inoperable)